Applied Organometallic Chemistry

Received: 23 July 2008 Accepted: 14 August 2008 Published online in Wiley Interscience: 22 September 2008

(www.interscience.com) DOI 10.1002/aoc.1458

AACVD of WO_3 thin films from $W(O)(OPr^i)_3[O(CH_2)_nNMe_2]$ ($n = 2, 3$)

K. C. Molloy* and P. A. Williams

Monomeric tungsten oxo-aminoalkoxides $W(O)(OPr^i)_3(L)$ [$L = O(CH_2)_nNMe_2$; $n = 2$ (dmae, 1) and 3 (dmap, 2)] were synthesized by alcohol exchange with $[W(O)(OPr^i)_4]_2$ and characterized spectroscopically. 1, 2 and $[W(O)(OPr^i)_4]_2$ were used as precursors for the aerosol-assisted chemical vapour deposition of WO_3 thin films, which were characterized by glancing angle X-ray diffraction, SEM and transmission-reflectance measurements.

Supporting information may be found in the online version of this article.

Keywords: CVD; thin film; tungsten oxide; single-source precursor; alkoxide

Introduction

Tungsten oxide is an important inorganic material with a number of key properties (electrochromism, photochromism, photocatalysis) that have translated to a diverse range of applications.[1] As a transparent conducting oxide (TCO) it is seen as a potential 'smart window', capable of controlling the absorbance of solar radiation as a function intensity and thus controlling interior lighting and temperature levels. With a band gap of 2.7 eV, conductance band electrons capable of reducing oxygen to water (E° −0.5 eV vs NHE) and valence band holes more oxidizing than TiO_2, it has potential as a photocatalytic coating that harvests more visible radiation than the widely studied titania.[2–4] Its conductivity also makes it applicable as a gas sensor, for example for NO_2, H_2S and O_3.[5]

The properties of tungsten oxide thin films are strongly dependent on the deposition technique and choice of precursor. Sol–gel,[6] sputtering[7] and spray pyrolysis[8] methods have been reported, but CVD offers the greatest potential for large-scale coatings. We have reported the use of $W(OR)_6$ (R = C_6H_5, C_6H_4F-4, $C_6H_3F_2$-3,4) precursors in this latter regard,[9] which compliments other studies involving tunsten(IV) halides,[10,11] various tungsten alkoxides [$W(OEt)_n$, $n = 5, 6$][12] and oxo-alkoxides [$W(O)(OR)_4$, R = Et, Pr^i, Bu^t, CH_2Bu^t],[13,14] and organometallic precursors such as $W(CO)_6$,[15] $W(CO)_4(PR_3)_2$ (R = OEt) or $W(\eta^3\text{-}C_3H_4)_4$.[16] More recently, the innovative use of poly-tungstates in an aerosol-assisted delivery route has been reported by Parkin.[17]

In this paper we report the synthesis of monomeric tungsten oxo-aminoalkoxides $W(O)(OPr^i)_3(L)$ [$L = O(CH_2)_nNMe_2$; $n = 2$ (dmae) and 3 (dmap)] and, along with $[W(O)(OPr^i)_4]_2$, their application as precursors for the CVD of WO_3 thin films. Previous attempts to control the precursor chemistry by the use of chelating ligands have been confined to one report on mixed alkoxide/β-diketonates $W(O)(OR)_3(L)$ (L = acac, hfac).[13]

Experimental

Elemental analyses were performed using a Carlo-Erba Strumentazione E.A. model 1106 microanalyser operating at 500 °C; results were calibrated against an acetanilide [$PhNHC(O)CH_3$] standard. ^1H and ^{13}C NMR spectra were recorded using either a Jeol JNM-GX-270FT (270 MHz) or a Jeol EX-400 (400 MHz) Fourier Transform spectrometer, while ^{183}W NMR spectra were recorded on a Jeol EX400 (400 MHz) machine. Chemical shifts are in ppm with respect to either Me_4Si (^1H, ^{13}C) or 1 mol dm^{-3} solution of Na_2WO_4/D_2O (^{183}W); coupling constants are in Hz. SEM was carried out on a Jeol JSM-6310 microscope equipped with Oxford Instruments ISIS EDXS attachment, XRD was performed using a Philips PW1130 generator operating at 45 kV and 40 mA to power a copper fine focus X-ray tube, in conjunction with a PW 1820 goniometer fitted with thin film optics and a proportional X-ray detector. The transmission and reflectance spectra of the coated samples (*ca* 2 cm square) were measured between wavelengths 240 and 2600 nm, inclusive, using a Hitachi u-4000 spectrometer calibrated with a rhodium mirror.

All synthetic manipulations were carried out under a nitrogen or argon atmosphere using standard Schlenk techniques or in a dry-box fitted with a recirculation system. Tetrahydrofuran, toluene and hexane were dried over, and distilled from, sodium-benzophenone immediately prior to use; Hdmae, Hdmap and propan-2-ol were purchased from Aldrich and dried over molecular sieves once opened. $[W(O)(OPr^i)_4]_2$ was prepared using a literature procedure.[18]

Synthesis of $W(O)(OPr^i)_3$(dmae) (1)

$[W(O)(OPr^i)_4]_2$ (3.30 g, 3.78 mmol) was dissolved in tetrahydrofuran (*ca* 60 ml) and 2 equivalents of Hdmae (0.67 g, 7.57 mmol) was added with stirring. The solution was then refluxed for 2 h and allowed to cool. Removal of all volatiles *in vacuo* gave a cloudy yellow oil which was then purified by vacuum distillation (100 °C at 0.1–0.2 mmHg) to give **1** as a clear pale yellow oil. Yield 1.69 g (48%). Analysis: found (calculated for $C_{13}H_{31}NO_5W$), C, 33.6 (34.2); H, 6.77 (4.85); N, 4.80 (3.07)%. NMR [δ (ppm), toluene-d^8 soln, 20 °C], ^1H: 1.36 [18H, m, $OCH(CH_3)_2$]; 2.39 [6H, s, $OCH_2CH_2N(CH_3)_2$]; 2.49

* *Correspondence to: K. C. Molloy, Department of Chemistry, University of Bath, Bath BA2 7AY, UK. E-mail: chskcm@bath.ac.uk*

Department of Chemistry, University of Bath, Bath BA2 7AY, UK

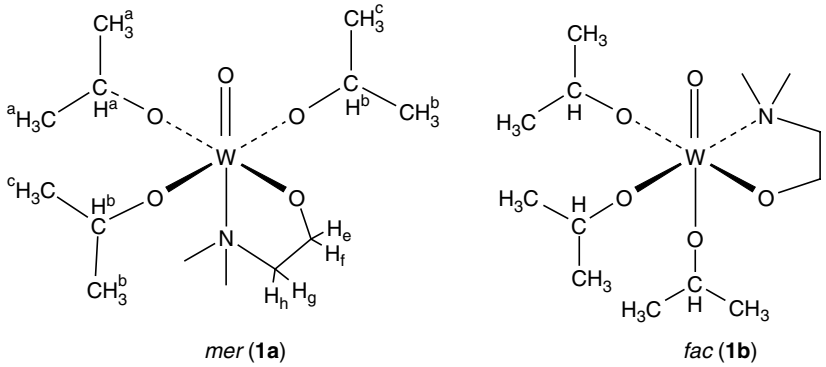

Scheme 1. Possible isomeric forms of six-coordinated **1**.

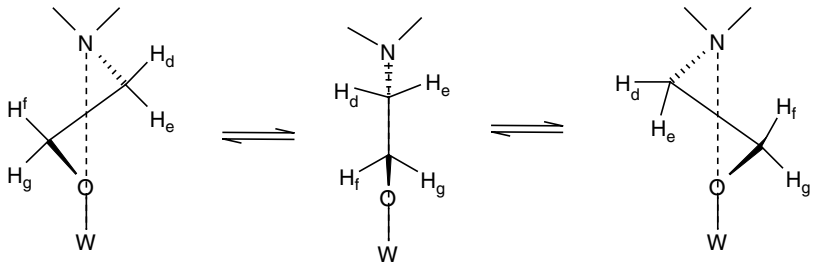

Scheme 2. "Windscreen wiper" mechanism for the equivalence of the methylene protons in dmae ligand of **1**, seen in the 60 °C ^{1}H NMR spectrum [Fig. 3(b)].

[2H, m, $OCH_2CH_2N(CH_3)_2$]; 4.53 [2H, m, $OCH_2CH_2N(CH_3)_2$]; 4.95 [3H, m, $OCH(CH_3)_2$]; ^{13}C: 23.7 [$OCH(CH_3)_2$]; 24.1 [$OCH(CH_3)_2$]; 46.8 [$OCH_2CH_2N(CH_3)_2$]; 61.4 [$OCH_2CH_2N(CH_3)_2$]; 61.7 [$OCH_2CH_2N(CH_3)_2$]; 67.6 [$OCH_2CH_2N(CH_3)_2$]; 75.8 [$OCH(CH_3)_2$]; 76.0 [$OCH(CH_3)_2$]; 76.1 [$OCH(CH_3)_2$]; ^{183}W: −88.5. IR data (NaCl plates, cm^{-1}): 3013, 2966, 2926, 2865, 2817, 2792, 2769, 1455, 1404, 1375, 1376, 1330, 1272, 1256, 1244, 1165, 1113, 1050, 1022, 969, 897, 842, 782, 754, 597.

Synthesis of $W(O)(OPr^i)_3$(dmap) (2)

Compound **2** was prepared *via* a similar method to that used for **1**. $[W(O)(OPr^i)_4]_2$ (4.00 g, 4.59 mmol) and two equivalents of Hdmap (0.95 g, 9.17 mmol) were used in freshly distilled tetrahydrofuran (*ca* 60 ml). Once the reaction was complete and the volatiles removed, the product was obtained by vacuum distillation (98 °C at 0.2–0.3 mmHg) in the form of a clear pale yellow oil. Yield 2.15 g (49%). Analysis: found (calculated for $C_{14}H_{33}NO_5W$), C, 34.6 (35.0); H, 6.87 (6.94); N, 3.53 (2.92). NMR [δ (ppm), toluene-d^8 soln, 20 °C], ^{1}H: 1.32 [18H, m, $OCH(CH_3)_2$]; 1.41 [2H, m, $OCH_2CH_2CH_2N(CH_3)_2$]; 2.17 [6H, s, $OCH_2CH_2CH_2N(CH_3)_2$]; 2.31 [2H, m, $OCH_2CH_2CH_2N(CH_3)_2$]; 4.53 [2H, m, $OCH_2CH_2CH_2N(CH_3)_2$]; 5.00 [3H, m, $OCH(CH_3)_2$]; ^{13}C: 24.6 [$OCH(CH_3)_2$]; 24.9 [$OCH(CH_3)_2$]; 28.1 [$OCH_2CH_2CH_2N(CH_3)_2$]; 48.9 [$OCH_2CH_2CH_2N(CH_3)_2$]; 60.7 [$OCH_2CH_2CH_2N(CH_3)_2$]; 72.1 [$OCH_2CH_2CH_2N(CH_3)_2$]; 76.6 [$OCH(CH_3)_2$]. IR data (NaCl plates, cm^{-1}): 3015, 2966, 2930, 2864, 2837, 2788, 2722, 1463, 1375, 1369, 1331, 1260, 1244, 1230, 1165, 1109, 1061, 1002, 969, 843, 776, 567.

AACVD Experiments

Films were deposited using aerosol-assisted CVD (AACVD) on a 4 mm glass substrate undercoated with a thin film of SiCO which acts as a blocking layer to prevent sodium diffusion into the deposited film. Precursors [**1, 2** and $W(O)(OPr^i)_4$ (**3**)] were dissolved in toluene (freshly distilled over sodium-benzophenone) and transported to the reactor in an aerosol by nitrogen carrier gas; no additional oxygen was added to the reactive gas stream; experimental details are given in Table 1. Details of the horizontal cold-wall reactor used during these experiments can be found elsewhere.[19]

Table 1. Conditions used for AACVD using precursors **1, 2** and $[W(O)(OPr^i)_4]_2$ (**3**)

Precursor	1	2	3
Film ID	R1	R2	R3
Concentration (g cm^{-3})	0.01	0.01	0.02
Substrate temp (°C)	400	450	450
Carrier gas (N_2) flow rate (l min^{-1})	1.0	1.2	1.0
Run time (min)	22	12	30
Film thickness (Å)	8500[a]	3460[b]	8170[c]

[a] ±40; [b] ±90; [c] ±300;

Results and Discussion

Synthesis

Donor-functionalized tungsten(VI) oxo-aminoalkoxides were synthesized by the reaction of 2 equivalents of the appropriate chelating ligand (Hdmae, Hdmap) with dimeric $[W(O)(OPr^i)_4]_2$ in THF. The reaction mixture was refluxed for *ca* 2 h to ensure the reaction was complete before the solvent and volatiles were

removed *in vacuo*.

$$[W(O)(OPr^i)_4]_2 + 2Me_2N(CH_2)_nOH \xrightarrow[-2\ HOPr^i]{THF} 2W(O)(OPr^i)_3[O(CH_2)_nNMe_2)]n = 2(\mathbf{1}), 3(\mathbf{2}).$$

The waxy yellow oils recovered were vacuum distilled to yield (*ca* 50%) the products as pale yellow, air- and moisture-sensitive oils. One attempt was made to substitute two of the isopropoxide ligands for two dmae ligands via the same methodology; however, the ^{1}H NMR spectrum of the recovered compound indicated the presence of only one dmae ligand.

Spectroscopy

^{1}H NMR spectrum for **1** (Fig. 1) showed the expected peaks for the dmae ligand at 4.53 ppm [$OCH_2CH_2N(CH_3)_2$], 2.49 ppm [$OCH_2CH_2N(CH_3)_2$] and 2.39 ppm [$OCH_2CH_2N(CH_3)_2$], and multiplets at 4.95 ppm [$OCH(CH_3)_2$] and 1.36 ppm [$OCH(CH_3)_2$] from the OPr^i groups. The integrals from these peaks indicated that one dmae ligand had replaced one OPr^i ligand, as expected. However, the spectrum is complex with overlapping doublets at 1.36 ppm and two (or three) overlapping septets at *ca* 4.95 ppm, indicative of multiple OPr^i environments. The two CH_2 signals from the dmae ligand also appear as multiplets.

Both variable temperature and variable concentration ^{1}H NMR experiments were performed on **1** at three different solution concentrations (50, 15, 5% w/v) and temperatures between −60 and +70 °C. Dilution was seen to move the shifts of the dmae protons by between 0.10 and 0.25 ppm to high field, with the largest shift associated with the CH_2N signal, while the isopropoxide signals underwent less pronounced shifts, though the CH proton was more concentration-dependent than the CMe protons. However, the general appearance of the major resonances remained unchanged. Also visible in the room temperature spectrum (Fig. 1) were three broad featureless regions at 2.25, 2.51 and 4.71 ppm, albeit of low intensity. These signals, arising from a dmae ligand, sharpened at −45 °C and were consistent with a second species present in solution. These resonances disappeared at high dilution, suggesting the possible presence of a dimeric species present at high concentrations.

The ^{183}W NMR spectrum recorded for **1** gave one peak at −88.6 ppm, consistent with other ^{183}W NMR chemical shift values recorded for six coordinate oxo-tetraalkoxide complexes ($[W(O)(OMe)_4]_2$ −62.9 ppm); for comparison, five-coordinated $W(O)(OBu^t)_4$ has as ^{183}W shift of −386.9 ppm.[18] Thus, both a bridging alkoxide and, simultaneously, a chelated aminoalkoxide can be ruled out as this would require a seven-coordinate metal. The starting reagent $[W(O)(OPr^i)_4]_2$ is an OPr^i-bridged dimer, and we have shown that unfunctionalized alkoxides can bridge in the presence of aminoalkoxides even if the latter are forced on occasion to become monodentate themselves, e.g. $[Ti(OEt)_3(dmae)]_2$,[20] so a dimeric structure for **1** is plausible. However, a six-coordinated tungsten, as indicated by the ^{183}W NMR, is most easily accommodated by one of the isomeric monomers **1a, 1b** (Scheme 1).

There are two [$OCH(CH_3)_2$] signals at *ca* 4.9 ppm in the ratio of 2 : 1 and a group of signals for the [$OCH(CH_3)_2$] protons at *ca* 1.36 ppm (inset, Fig. 1). In the *mer* configuration two of the [$OCH(CH_3)_2$] protons (H_b) are equivalent and the third is not (H_a), giving rise to the 2 : 1 ratio seen in the ^{1}H NMR spectra.

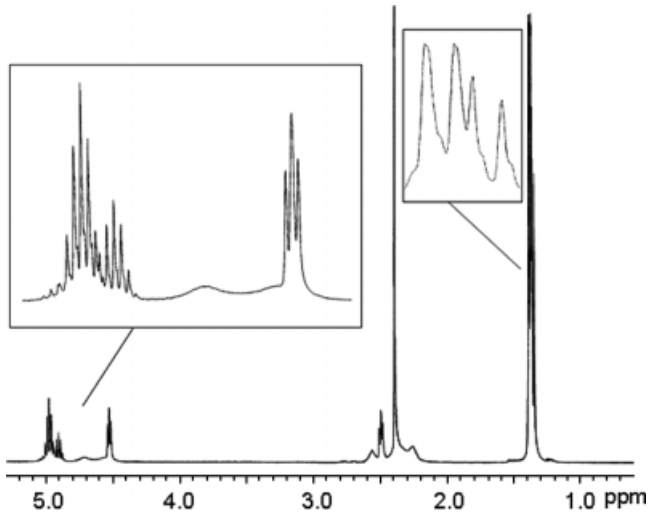

Figure 1. ^{1}H NMR spectra recorded for **1** at 20 °C and 25% w/v concentration.

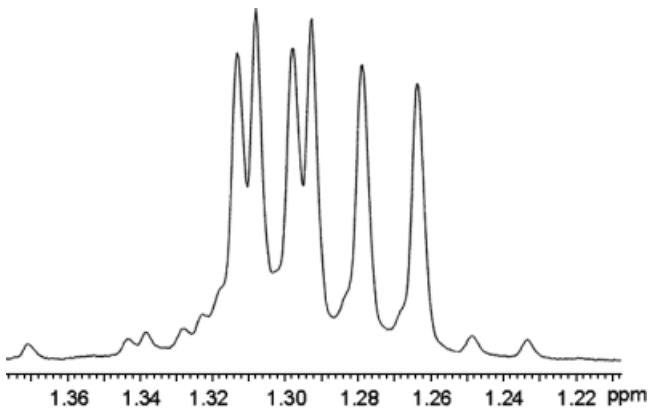

Figure 2. Enlargement of methyl region of ^{1}H NMR spectra of **1a** recorded at 30 °C with a solution concentration of 15% by volume.

The lower symmetry *fac* isomer (**1b**) can be eliminated on this basis. If the *mer* configuration is adopted by the molecule then the methyl groups which couple with H_b are not equivalent, which would give rise to a quartet of quartets for the H_b signal. However, the coupling constants between H_b and the two sets of methyl protons are likely to be very similar, leading to the apparent septet observed. There are three types of methyl group present in the *mer* isomer (**1a**), in the ratio of 1 : 1 : 1. At 20 °C/15% concentration these signals are not fully resolved (inset, Fig. 1); however at 30 °C the three doublets arising from the methyl protons [$OCH(CH_3)_2$] are clearly visible (Fig. 2). This also suggests that the N: → W bond is persistent and not undergoing the rapid breaking and reformation which would allow a scrambling of the OPr^i groups.

While the *N*-methyl groups appear equivalent, signals for the methylene groups of the dmae ligand (*ca* 4.5, OCH_2 and *ca* 2.5 ppm, CH_2N) are more complex and showed that H_d–H_g are non-equivalent [Fig. 3(a)]. Equivalence occurred at 60 °C [Fig. 3(b)], evidenced by coalescence to a simple triplet, consistent with a 'windscreen wiper'-type motion of the ethylene moiety (Scheme 2).

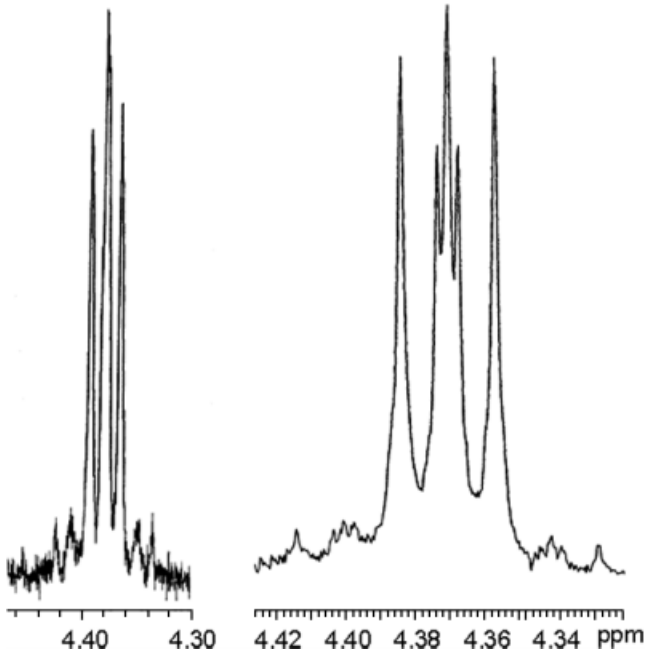

Figure 3. ^{1}H NMR spectra due to (a) OCH_2 recorded at 15 °C (right) and (b) 60 °C (left) for **1a** with a solution concentration of 5% by volume.

At 70 °C, a 50% by volume solution shows close to a single septet for the $[OCH(CH_3)_2]$ protons and the $[OCH(CH_3)_2]$ signals collapsing to almost a simple doublet. Additionally, extra signals are seen for the dmae ligand at 4.60, 2.57 and 2.45 ppm which are two triplets and a singlet for the $[(OCH_2CH_2N(CH_3)_2]$, $[(OCH_2CH_2N(CH_3)_2]$ and $[(OCH_2CH_2N(CH_3)_2]$ protons, respectively. This data would seem to indicate that at high temperatures **1** is breaking the N: → W bond, which has the effect of rendering the OPr^i groups on the molecule equivalent. The additional dmae signals might have arisen from the generation of some *fac*-**1b** under these conditions.

In summary, while the behaviour of **1** in solution is complex and not fully understood across the whole temperature and concentration range, the ^{1}H VT NMR is consistent with a monomeric species which adopts a *mer* configuration (**1a**) dominating in solution. Compound **1** seems rigid at room temperature, and equivalence of OPr^i groups only occurs at elevated temperatures. This is in contrast to other compounds in the literature using dmae as a ligand, as these have shown the N: → M bond to be breaking and reforming to scramble the alkoxide signals at lower temperatures, most notably for $Ta(OEt)_5$(dmae).[21] While the possibility of dimeric species in solution cannot be fully excluded, they are likely to be present in very small amounts, if at all.

The ^{1}H NMR spectra of **2** showed the resonances expected for the dmap ligand (1.41, $CH_2CH_2CH_2$; 2.17, NCH_3; 2.31, CH_2N; 4.53 ppm, OCH_2), and at 1.32 and 5.00 ppm for the OPr^i groups. The integrals of these peaks showed that one dmap ligand had replaced one OPr^i ligand in the course of the reaction. However, as with **1**, the multiplicities of the resonances due to the dmap ligand are complex, though the OPr^i peaks appear as almost a simple doublet and a septet. Additionally, there are again broad humps at 1.64, 2.34 and 4.63 ppm, in addition to a sharp peak at 2.14, the positions and integrals of which are consistent with a second dmap-containing species, again in parallel to **1**.

AACVD Testing of Precursors

LPCVD experiments have previously been carried out using dimeric $[W(O)(OPr^i)_4]_2$ (**3**),[18] which sublimes at 85–90 °C/0.01 mmHg. Reaction of **3** with the aminoalcohols Hdmae and Hdmap generated monomers, as viscous liquids distilling at 95–115 °C/*ca* 0.1–0.3 mmHg, representing a marginal increase in volatility. APCVD experiments were hampered by the low carry-over of the precursor, despite their liquid nature. Consequently, a comparative study of all three precursors was made using AACVD, where a high volatility is not a requirement (Table 1).

High-temperature (≥400 °C) deposition experiments were conducted on all three compounds synthesized during this study. Lower-temperature deposition experiments (365 °C) were also conducted on all three compounds synthesized. Films could be grown from **3** at temperatures as low as 260 °C; however, since the film deposited at 450 °C (R3) was barely crystalline, no analysis has been conducted on the low-temperature deposition runs from this precursor. Similarly, films grown from **1** and **2** at 365 °C were similar, but of lower crystallinity to those grown at higher temperatures.

Film R3, deposited using precursor **3**, had a black surface layer, probably carbon from solvent used to create the aerosol, which could be easily removed on wiping leaving a deep blue film, suggestive of W(V) in a sub-stoichiometric WO_x, complete with coloured interference fringes. This film only covered the first third of the glass substrate (as opposed to the whole substrate when precursors **1**and **2** were employed). The colour of this film appeared stable in the atmosphere and after several months the film was still blue in colour.

The glancing angle X-ray diffraction pattern obtained for R3 [Fig. 4(a)] shows a large hump between 15 and 30° that is indicative of an amorphous component. While this could be sampling of the glass substrate, the film appeared thick, as indicated by coloured optical interference fringes, which were clearly evident from a visual analysis of the film, and from subsequent SEM measurements. There is also some evidence for a low level of crystalline tungsten oxide, as indicated by the small, superimposed peaks at *ca* 23°, typical of either crystalline stoichiometric WO_3 or non-stoichiometric $WO_{2.9}$. Given that the film was deposited in the absence of oxygen, and its intense blue colour, there is certainly some non-stoichiometric $WO_{2.9}$ present in the film composition. The amorphous nature of this film is somewhat surprising given the elevated deposition temperature (450 °C), and in contrast to films deposited at similar temperatures from precursors **1** and **2**, which were crystalline.

Films R1 and R2, derived from precursors **1** and **2** respectively, covered the full length of the glass substrate and, like R3, had a soft black surface layer which could be easily removed with a soft tissue leaving a well-adhered blue film with coloured interference fringes clearly visible. While initially blue in colour, these films were seen to slowly change colour on standing in the atmosphere. After 3–4 weeks areas on the edges of the films were yellow in colour, consistent with some aerobic oxidation to stoichiometric WO_3, although the bulk film was still blue. After 6–8 months the majority of the films were yellow rather than blue in colour; however, the coloured interference fringes were still evident. The glancing angle X-ray diffraction data displayed here were collected some months after the films were deposited, and while the bulk of the films were still blue, areas of yellow on the films were clearly evident.

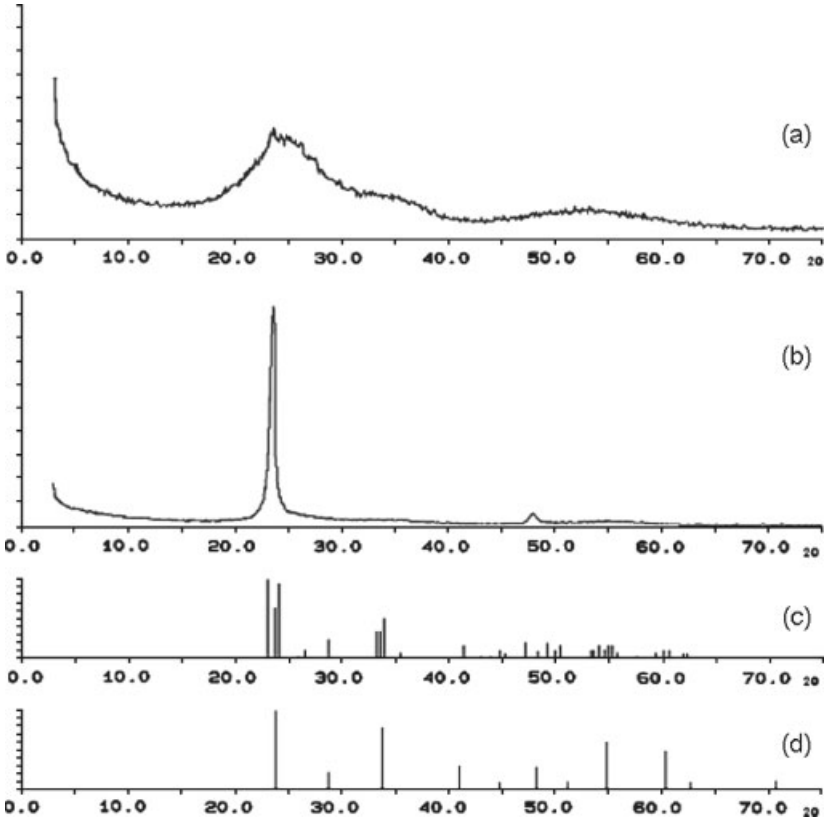

Figure 4. XRD of the films deposited from (a) **3** (R3) and (b) **1** (R1). Literature data are also shown for (c) randomly oriented WO_3 (PDF 20–1324) and (d) randomly oriented $WO_{2.9}$ (PDF 18–1417).

Glancing angle X-ray diffraction of the two high temperature deposition experiments (R1 and R2) gave identical diffraction patterns, typified by that for **1** [Fig. 4(b)], which indicated the films were crystalline and composed of tungsten oxide. Both these diffraction patterns are dominated by a single peak (index 110), which indicates a highly oriented crystalline structure.

When deposited the films were intensely blue in colour, characteristic of non-stoichiometric $WO_{2.9}$; however, on standing in the atmosphere over several weeks the blue colour faded on the thinner areas of the films to give a yellow colour, characteristic of stoichiometric WO_3. It is therefore not unreasonable to suggest that the glancing angle X-ray diffraction patterns could contain both $WO_{2.9}$ and WO_3 phases and peak match software is superficially consistent with both non-stoichiometric tetragonal $WO_{2.9}$ (PDF 18–1417) and/or stoichiometric orthorhombic WO_3 (PDF 20–1324). However, the evidence for the presence of significant amounts of crystalline stoichiometric WO_3 is not strong. The line from the WO_3 reference sample (PDF 20–1324) which aligns with the main observed diffraction peak (020, at 23.7°) is the least intense of the group of three closely spaced lines in the reference diffraction pattern; additionally, no other peaks seen in the reference pattern are visible in the experimental diffraction pattern. The only other peak seen in the diffraction pattern (48.4°) is best matched to the (220) line in the non-stoichiometric $WO_{2.9}$ reference sample (PDF 18–1417). Since the films were initially blue in colour, and were deposited in the absence of an oxygen source, both R1 and R2 appear to be entirely non-stoichiometric $WO_{2.9}$ with preferred orientation in the 110 direction when first removed from the reactor.

The morphology of the films has been probed by SEM. Figure 5 shows the film deposited from $[W(O)(OPr^i)_4]_2$ (R3) at differing tilt angles. Figure 5(a) clearly shows the glass substrate surface, the SiCO undercoat and then the tungsten oxide film that has been deposited. The surface of the deposited film appears rough, possibly grown *via* an island growth method, and bears a resemblance to the film grown from $W(O)(OBu^t)_4/H_2O$ under sol–gel conditions.[14] The surface roughness can also be clearly seen in Fig. 5(b), which also indicates a columnar structure to the film, despite its amorphous nature.

Figure 6 shows the film deposited from **1** (R1) from the same angles and magnifications as R3. The structure and surface morphology of R1, in contrast to R3, is smooth, uniform and without micro-domains. The film deposited from **2** (R2) is virtually the same in appearance as that from **1**, though with a greater surface roughness (Fig. 7). This increase in surface roughness could have been caused by cleaning, transportation or storage of the film rather than being a natural feature. However, there appears to be greater structural detail than is seen in the corresponding image for R1 (Fig. 6).

Transmission–Reflectance Spectra

The transmission–reflectance spectra were recorded for all three films, where:

$$\text{Absorption} = 100\% - (\text{transmission} + \text{reflectance})$$

For solar control applications good film transmission is required in the solar spectrum (350–780 nm) and for it to either absorb or reflect at longer wavelengths (780–2000 nm).[22]

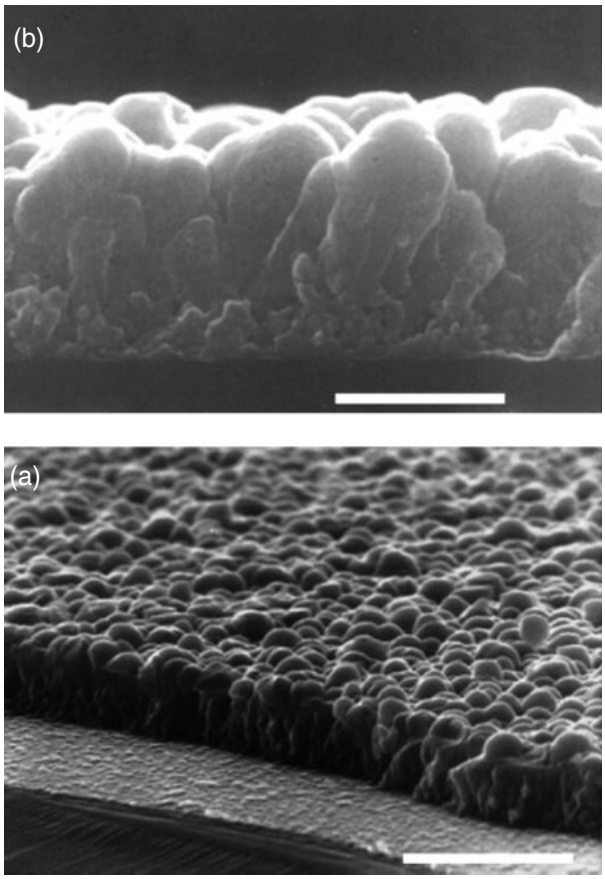

Figure 5. SEM images from film deposited from **3** at 450 °C (R3): (a) 80° tilt (bar = 1.5 μm); (b) 90° tilt (bar = 600 nm).

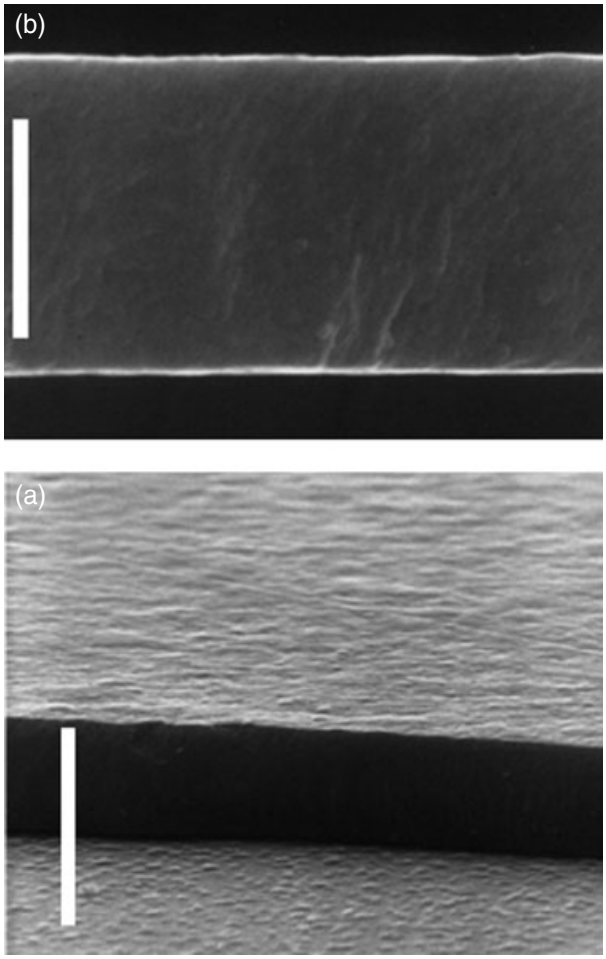

Figure 6. SEM images from film deposited from **1** at 400 °C (R1): (a) 80° tilt (bar = 1.5 μm); (b) 90° tilt (bar = 600 nm).

Figure 8 displays the spectra recorded from R3. SEM analysis has shown the surface of this film to be relatively rough when compared with R1 and R2; however, its thickness is comparable to R1. The maximum visible transmission is approximately 56% at 460 nm and the transmission then falls sharply to a minimum of 23% at 1000 nm before rising again to 63% at approximately 2350 nm. The fall in the transmission of radiation is mirrored by a rise in absorption over the same region, demonstrating that the film is absorbing the radiation rather than reflecting it. There is a small (10%) rise in the reflectance between 1000 and 2000 nm. The region of high absorption and low transmission (590–1600 nm) demonstrates that the film is showing some selectivity to the solar spectrum in the infrared region; however, this does extend into the visible portion of the spectrum and the maximum visible transmission is poor.

The transmission–reflectance–absorption of the film deposited from **1** is shown in Fig. 9. The film is highly absorbing with the maximum transmission of visible radiation being only 27% at 475 nm. This poor transmission is in contrast to the film derived from **3**, which is also over 8000 Å thick and clearly possesses a much rougher surface. The selectivity in the transmission curve over the infrared region of the solar spectrum is mirrored in the calculated absorption curve, demonstrating that the coating is absorbing the infrared energy as opposed to reflecting it. Thus, despite the relatively poor visible transmission from this film, it still displays characteristics consistent with solar control applications.

The transmission–reflectance–absorption spectra of the film from deposition using precursor **2** show that transmission in the visible region is relatively poor (43% at 550 nm) and, while there is subsequently a fall in the transmitted radiation, it only amounts to a 7% reduction. The absorption curve displays a small increase in the infrared region of the solar spectrum, showing the film does have some selectivity to the solar spectrum; however, the properties shown are the most disappointing for the three films deposited.

The superior optical properties of the amorphous film derived from **3** in comparison to the two crystalline films from **1** and **2** are consistent with an earlier report that also notes that amorphous films (usually deposited at $T < ca$ 300 °C to avoid crystallization) have better electrochromic properties than polycrystalline films.[14]

Summary

We have synthesized two tungsten compounds [$W(O)(OPr^i)_3(L)$, L = dmae, dmap] using donor-functionalized alkoxide ligands to break up the dimeric structure of tungsten(VI) oxo-tetraalkoxides and hence generate an increase in volatility, albeit only marginally. Monomeric, six-coordinated species seem dominant in solution on the basis of ^{183}W NMR and ^{1}H VT NMR techniques, but the

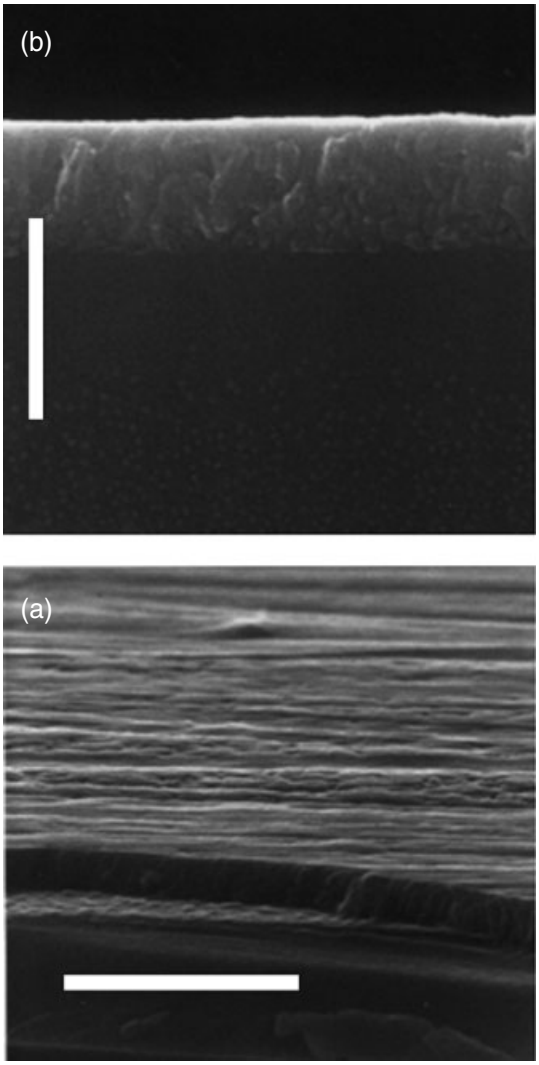

Figure 7. SEM images from film deposited from **2** at 450 °C (R2): (a) 80° tilt (bar = 1.5 μm); (b) 90° tilt (bar = 600 nm).

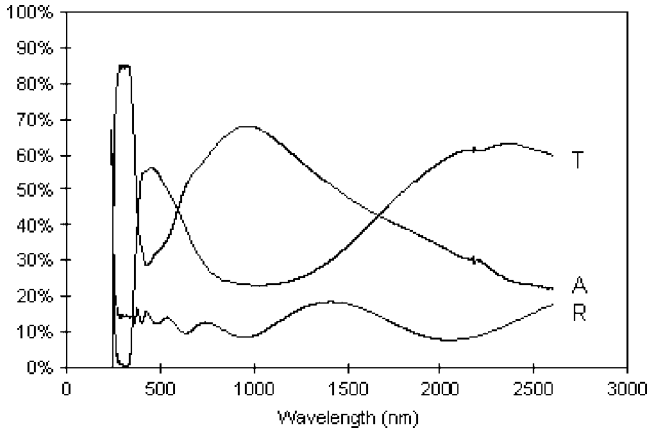

Figure 8. Transmission–reflectance–absorption spectra recorded for **3** (R3).

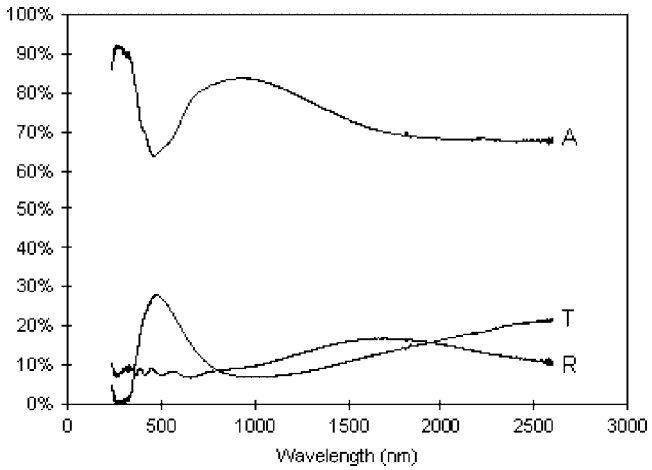

Figure 9. Transmission–reflectance–absorption spectra recorded for **1** (R1).

presence of higher aggregates in more concentrated solutions cannot be discounted. Non-stoichiometric $WO_{2.9}$ films were deposited from the synthesized compounds in a single-step deposition process via AACVD and showed some selectivity to solar radiation; however, their transmission of visible light was generally poor. $[W(O)(OPr^i)_4]_2$ can also be used to deposit films of non-stoichiometric $WO_{2.9}$, though unlike the films deposited from the novel precursors this film is largely amorphous. However, it did show the most promising optical spectra from a solar control perspective.

Acknowledgements

We thank the EPSRC and Pilkington plc for support in the form of a CASE studentship (to P.A.W.).

Supporting information

Supporting information may be found in the online version of this article.

References

[1] P. M. S. Monk, R. J. Mortimer, M. J. Rosseinsky, *Electrochromism: Fundamentals and Applications*. VCH: New York, **1995**.
[2] S. H. Baeck, K. S. Choi, T. F. Jaramillo, G. D. Stucky, E. W. McFarland, *Adv Mater.* **2003**, *15*, 1269.
[3] S. Ikeda, T. Itani, K. Nango, M. Matsumura, *Catal. Lett.* **2004**, *98*, 229.
[4] B. Yang, P. R. F. Barnes, Y. Zhang, V. Luca, *Catal. Lett.* **2007**, *118*, 280.
[5] K. Zakrzewka, *Thin Solid Films* **2001**, *391*, 229.
[6] C. O. Avellaneda, L. O. S. Bulhoes, *Solid-St. Ionics* **2003**, *165*, 117.
[7] M. Ferroni, V. Guidi, E. Comini, G. Sberveglieri, A. Vomiero, G. Della Mea, G. Martinelli, *J. Vac. Sci. Technol.* **2003**, *21*, 1442.
[8] M. Regragui, M. Addou, B. El Idrissi, J. C. Bernede, A. Outzourhit, E. Ec-chamikh, *Mater. Chem. Phys.* **2001**, *70*, 84.
[9] W. B. Cross, I. P. Parkin, S. A. O'Neill, P. A. Williams, M. F. Mahon, K. C. Molloy, *Chem. Mater.* **2003**, *15*, 2786.
[10] T. Kodas, M. J. Hampden-Smith, *The Chemistry of Metal CVD*. VCH: Weinheim, **1994**.
[11] S. Ashraf, R. Binions, C. S. Blackman, I. P. Parkin, *Polyhedron* **2007**, *26*, 1493.
[12] U. Riaz, *Thin Solid Films* **1993**, *235*, 15.
[13] D. V. Baxter, M. H. Chisholm, S. Doherty, N. E. Gruhn, *J. Chem. Soc., Chem. Commun.* **1996**, 1129.
[14] M. Basato, E. Brescacin, E. Tondello, *Chem. Vap. Deposition* **2001**, *7*, 219.
[15] S. Ashraf, C. S. Blackman, R. G. Palgrave, S. C. Naisbitt, I. P. Parkin, *J. Mater. Chem.* **2007**, *17*, 3708.

[16] L. Meda, R. C. Breitkopf, T. E. Haas, R. U. Kirss, *Thin Solid Films* **2002**, *402*, 126.
[17] S. Ashraf, C. S. Blackman, R. G. Palgrave, I. P. Parkin, *J. Mater. Chem.* **2007**, *17*, 1063.
[18] W. Clegg, R. J. Errington, P. Kraxner, C. Redshaw, *J. Chem. Soc., Dalton Trans.* **1992**, 1431.
[19] D. A. Edwards, R. M. Harker, M. F. Mahon, K. C. Molloy, *J. Mater. Chem.* **1999**, *9*, 1771.
[20] N. Hollingsworth, M. Kanna, G. Kociok-Köhn, K. C. Molloy, S. Wongnawa, *Dalton Trans.* **2008**, 631.
[21] H. O. Davies, T. J. Leedham, A. C. Jones, P. O'Brien, A. J. P. White, D. J. Williams, *Polyhedron* **1999**, *18*, 3165.
[22] C. G. Granqvist, *Sol. Energy Mater.* **2007**, *91*, 1529.

